On the Electronic Structure of the New "Intermetallics" $LnNi_2B_2C$

Gordon J. Miller

Contribution from the Department of Chemistry, Iowa State University, Ames, Iowa 50011

Received February 18, 1994. Revised Manuscript Received April 19, 1994•

Abstract: The electronic structure of the new series of intermetallic compounds $LnNi_2B_2C$ (Ln = lanthanide element) is calculated and discussed in terms of local chemical bonding in order to elucidate how superconductivity may be possible for some of these materials. The Fermi level occurs in a region that allows for a second-order Jahn–Teller mixing and can contribute to significant electron–phonon coupling in these systems. Moreover, the trend in the *a* lattice parameter for different Ln cations shifts the position of the x^2-y^2 band, which significantly changes its occupation and affects the superconducting transition temperature. We also compare the electronic structures of $LnNi_2B_2C$ with those from the related compounds LnNiBC.

Recent reports of superconducting transition temperature (T_cs) ranging from 8.0 to 16.6 K in quaternary "intermetallics" $LnNi_2B_2C$ (Ln = Ho, Er, Tm, Y, Lu) will undoubtedly lead to numerous investigations in this compound class.[1] As Cava and co-workers remark, "working with more complex chemical systems allows greater opportunity to balance opposing forces within a single chemical compound, leading to a better optimization of physical properties". The questions arise, therefore, regarding the nature of these "opposing forces" within the series $LnNi_2B_2C$, and how they may affect the observed superconductivity for some of them. In order to assess how this structure allows a relatively high T_c, we have carried out tight-binding electronic structure calculations within the Extended Hückel approximation[2] on the series $LnNi_2B_2C$ (see Appendix for details of the calculations).

Mechanisms of superconductivity have undergone tremendous scrutiny since the discovery of high T_cs in cuprate systems,[3] but conventional pictures arising from the Bardeen–Cooper–Schrieffer (BCS) theory incorporate electron–phonon interactions to promote a pairing mechanism between electrons with opposite crystal momenta that leads to a superconducting state.[4] The qualitative correlation arising between T_c and the density of states (DOS) at the Fermi level, $N(E_F)$, is $kT_c = 1.13\hbar\omega \exp(-1/N(E_F)V)$, where V is a measure of the electron–phonon interaction and ω is a characteristic phonon frequency whose magnitude is similar to the Debye frequency.[5] According to this expression, large values of either $N(E_F)$ or V (or both) lead to high T_c values. Superconductors among the early transition-metal carbides and nitrides and the well-known A15 compounds (Nb_3Sn, for example), whose T_cs can reach ca. 25 K, show either high values of V (carbides, nitrides) or high values of $N(E_F)$ (A15 compounds).[6]

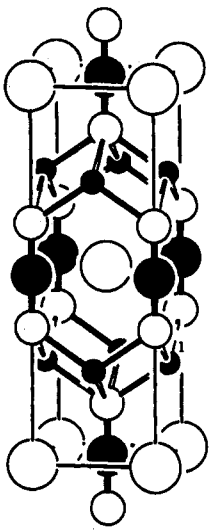

1

The structure of these new quaternary materials is a fascinating variant of the exceedingly popular intermetallic $ThCr_2Si_2$[7] (see **1**). In $LuNi_2B_2C$,[8] for example, C atoms (large filled circles) insert themselves between adjacent B (small open circles) atoms to give linear BCB trimers oriented parallel to the tetragonal *c* axis (B–C ≈ 1.47 Å). The Ni atoms (small filled circles) form square nets (Ni–Ni ≈ 2.45 Å) and are tetrahedrally coordinated by B atoms (Ni–B ≈ 2.10 Å; B–Ni–B angles ≈ 108.8° and 110.9°). As Siegrist et al. point out, this structure represents the first member of a homologous series $(LnC)_n(Ni_2B_2)$, in which the LnC substructure adopts a NaCl-type arrangement.[8]

Electronic Structure of $LnNi_2B_2C$

The electronic structure of $ThCr_2Si_2$-type materials has been extensively examined in recent years.[9] As a particular example, Zheng and Hoffmann constructed the DOS for ternary 3d metal phosphides (AM_2P_2; A = alkaline earth element) in a series of

• Abstract published in *Advance ACS Abstracts*, June 1, 1994.

(1) Cava, R. J.; Takagi, H.; Zandbergen, H. W.; Krajewski, J. J.; Peck, Jr., W. F.; Siegrist, T.; Batlogg, B.; van Dover, R. B.; Felder, R. J.; Mizuhashi, K.; Lee, J. O.; Eisaki, H.; Uchida, S. *Nature* **1994**, *367*, 252.

(2) (a) Hoffmann, R. *J. Chem. Phys.* **1963**, *39*, 1397. (b) Whangbo, M.-H.; Hoffmann, R. *J. Am. Chem. Soc.* **1978**, *100*, 6093. (c) Ammeter, J.; Bürgi, H.-B.; Thibeault, J. C.; Hoffmann, R. *J. Am. Chem. Soc.* **1978**, *100*, 3686.

(3) For example: (a) Rice, T. M. *Z. Phys. B* **1987**, *67*, 141. (b) Pickett, W. E. *Rev. Mod. Phys.* **1989**, *61*, 433. (c) Mattheiss, L. F.; Hamann, D. R. *Phys. Rev. B* **1989**, *40*, 2217. (d) Burdett, J. K. *J. Solid State Chem.* **1992**, *100*, 393.

(4) (a) Ashcroft, N. W.; Mermin, N. D. *Solid State Physics*; Saunders College: Philadelphia, PA, 1976; Chapter 34. (b) Callaway, J. *Quantum Theory of the Solid State, Student Ed.*; Academic Press, Inc.: London, 1974; pp 662–697.

(5) McMillan, W. L. *Phys. Rev.* **1968**, *167*, 331.

(6) Toth, L. E. *Transition Metal Carbides and Nitrides*; Academic Press: New York, 1971; p 215.

(7) (a) Villars, P.; Calvert, L. D. *Pearson's Handbook of Crystallographic Data for Intermetallic Phases*; American Society for Metals: Metals Park, OH, 1985. (b) Pearson, W. B. *J. Solid State Chem.* **1985**, *56*, 278.

(8) Siegrist, T.; Zandbergen, H. W.; Cava, R. J.; Krajewski, J. J.; Peck, Jr., W. F. *Nature* **1994**, *367*, 254.

(9) (a) Hoffmann, R. *Solids and Surfaces: A Chemist's View of Bonding in Extended Structures*; VCH Publishers: New York, 1988; p 55. Zheng, C.; Hoffmann, R. *J. Phys. Chem.* **1985**, *89*, 4175.

0002-7863/94/1516-6332$04.50/0

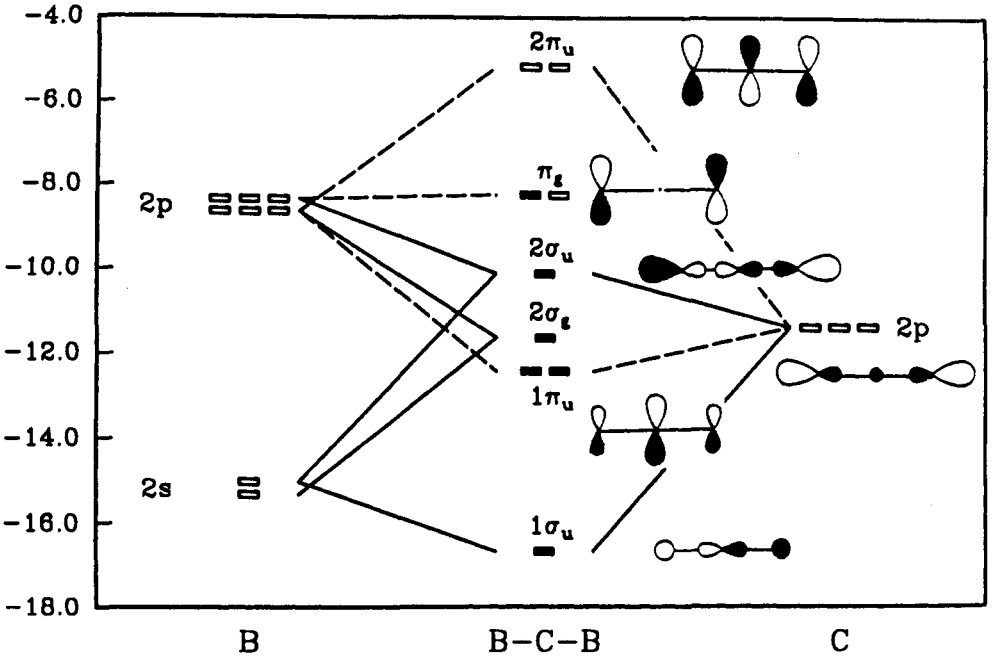

Figure 1. Molecular orbital interaction diagram for the linear B–C–B trimer observed in $LnNi_2B_2C$. Orbitals are labeled according to $D_{\infty h}$ local symmetry. Levels occupied for the $(BCB)^{3-}$ anion are darkened.

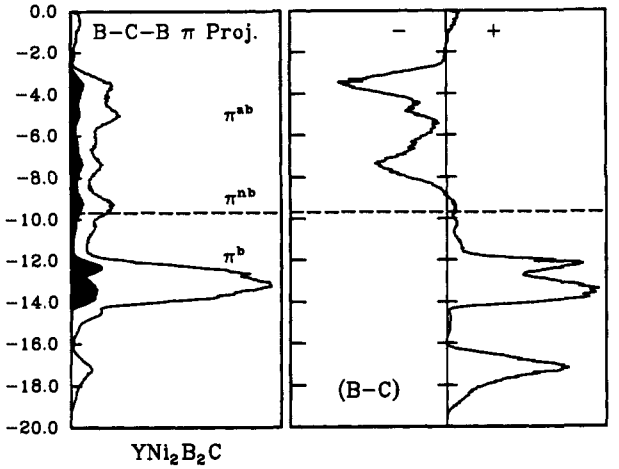

Figure 2. (Left) Total DOS and projection of the B–C–B π-type bands of YNi_2B_2C. The Fermi level at –9.68 eV is noted by a dashed line: (right) B–C COOP curve, (+) represents bonding interactions, and (–) indicates antibonding interactions. Integrated B–C COOP value at E_F is 0.99.

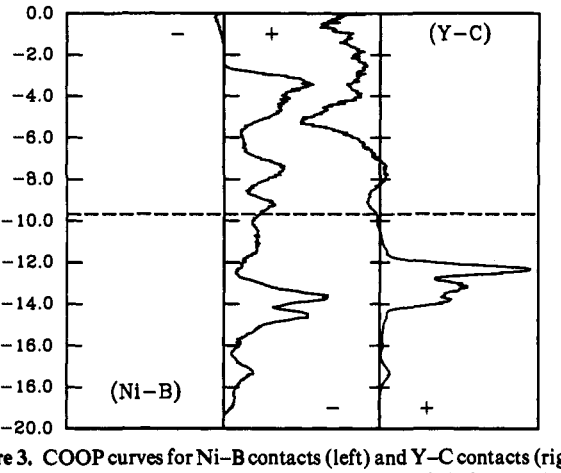

Figure 3. COOP curves for Ni–B contacts (left) and Y–C contacts (right) in YNi_2B_2C. Integrated COOP values at E_F are 0.17 (Ni–B) and 0.12 (Y–C).

steps and demonstrated how the position of the M 3d orbitals relative to the P–P σ^* fragment molecular orbital (MO) affected the observed P–P distance within the structure.[9] We shall utilize this general philosophy of linking molecular units together to form the three-dimensional extended solid to discuss the electronic structure of $LnNi_2B_2C$.

Since bond distances in $LnNi_2B_2C$ increase along the sequence B–C ≪ Ni–B < Ln–C, Ni–Ni < Ln–B < Ln–Ln, we shall treat the BCB trimer as a single chemical unit. Simple electron counting leads to the approximate ionic formulation $Ln^{3+}(Ni^0)_2(B_2C)^{3-}$. The local tetrahedral coordination at Ni suggests a d^{10} (or, perhaps, $d^{10-\delta}$) configuration and gives $(B_2C)^{(3+\delta)-}$. Figure 1 shows a qualitative molecular orbital diagram for the linear B–C–B unit. The highest occupied MO (HOMO) for 13 electrons is a π_g orbital that is exactly B–C π nonbonding because symmetry restricts any contribution from the C valence orbitals. Sandwiched between the π bonding ($1\pi_u$) and nonbonding (π_g) levels are two very weakly σ bonding orbitals ($2\sigma_g$ and $2\sigma_u$) with large components on the terminal B atoms. When these molecular fragments are condensed with Y and Ni atoms, how are these fragment orbitals affected?

In a complex quaternary system, an immediate concern of our semiempirical theory is how to relate the atomic orbital energies of Ni and the lanthanide element to the fragment MO energies of the trimer. Magnetic measurements, photoelectron spectroscopy, and electronic structure calculations on numerous borides suggest that charge transfer would occur from lanthanide to boron and from boron to nickel, with a large amount of back donation from nickel to boron.[10] Charge iteration of the Ni and Y parameters in YNi_2B_2C agrees with this description (see Appendix for details). Thus, the Ni 3d orbitals lie below the HOMO for the 13-electron B–C–B fragment, whereas the Y 4d and 5s orbitals are above this level.

The total DOS curve for YNi_2B_2C is illustrated in Figure 2 along with the projection of B–C π bands. Clearly, the electronic structure shows $LnNi_2B_2C$ to be metals, and the Fermi level falls near a peak in the total DOS, which suggests a significant band structure contributionn to the observed T_cs. The crystal orbital overlap population (COOP) for the B–C interactions indicates that the bands close to the Fermi level are nearly B–C nonbonding,

(10) (a) *Boron and Refractory Borides*; Matkovich, V. I., Ed.; Springer-Verlag: New York, 1977. (b) Castaing, J.; Danan, J.; Rieux, M. *Solid State Commun.* **1972**, *10*, 563. (c) Castaing, J.; Caudron, R.; Toupance, G.; Costa, P. *Solid State Commun.* **1969**, *7*, 1453. (d) Cadeville, M. *J. Phys. Chem. Solids* **1966**, *27*, 667.

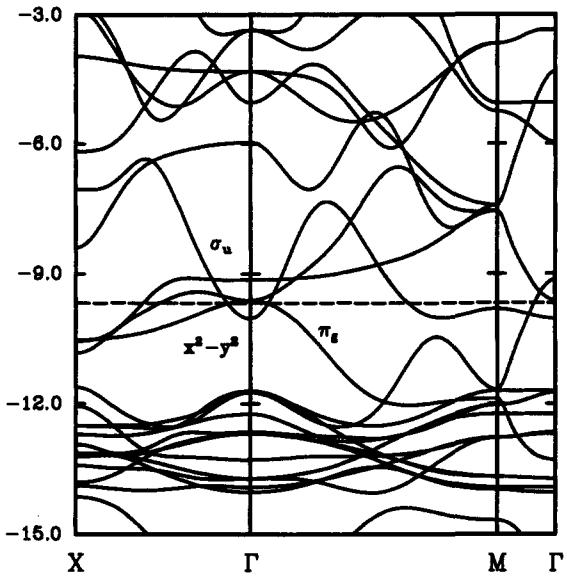

Figure 4. Energy band structure of YNi_2B_2C along three different directions of the FBZ for a body-centered tetragonal lattice:[14] Γ (0,0,0), *X* (1/2,0,0), *M* (1/2,1/2,0) *and* (0,0,1/2). Thus, the line ΓM is along [110] and MΓ is along [001] in the FBZ.

and, together with the DOS projection, suggest that there is a significant contribution from the π nonbonding orbital in the B–C–B fragment. This band occurs nearly 1.5 eV below the energy of the π_g B–C–B fragment orbital due largely (and perhaps surprisingly!) to Y–B interactions (see **2**) as well as a small attractive orbital overlap between Ni *x* and *y* orbitals with the B orbitals (not shown in **2** for clarity).

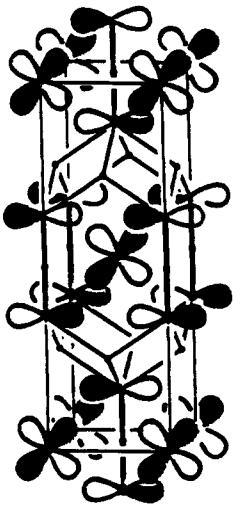

2

Decomposition of the total DOS into contributions from the various atomic components shows that Ni 3d orbitals as well as B–C–B σ and π bonding levels occur below –12.0 eV, with the Ni 3d orbitals largely concentrated between –14.0 and –12.0 eV in a fairly narrow band. Although the Ni–Ni separation of 2.45 Å is less than in the metal (2.50 Å), the relatively small overlap population of 0.0459 indicates only a weak attraction. Since the 3d band is formally filled and involves both bonding and antibonding overlap, this net interaction arises via mixing of valence 4s and 4p Ni orbitals into the occupied bands.[11] The short Ni–Ni distances within the square nets are the result of significant Ni–B orbital overlap. The COOP curves for both Ni–B and Y–C interactions are shown in Figure 3. Note the range of Ni–B bonding interactions around the Fermi level. Decomposition of the DOS reveals that these levels involve the $2\sigma_u$ B–C–B fragment orbital combined with Ni 3d, 4s, and 4p contributions. The resulting attractive interaction between Ni and B occurs when the higher energy 4s and 4p valence orbitals mix, via a bonding manner, into the antibonding combination of Ni 3d orbitals with the $2\sigma_u$ level. As we find in other lanthanide borocarbides,[12] the Y–C interactions are largely nonbonding in orbitals near the Fermi level, and all bonding levels are occupied.

The lanthanide cation's influence on the DOS near E_F is subtle, and the position of its valence d orbitals in the total spectrum depends critically on the size of the cation and their energy values in the free atom. As the cation varies from La to Lu in $LnNi_2B_2C$, *a* decreases and *c* increases nearly linearly as the ionic radii of the M^{3+} cations decrease.[8] Nevertheless, the unit cell volume decreases in consistent expectation with the lanthanide contraction.[13] For the later lanthanides with small *a* values, there is sufficiently positive overlap between adjacent x^2–y^2 orbitals to stabilize this crystal orbital (see **3**) at the Γ point (0,0,0) in the first Brillouin zone (FBZ) below the B–C–B π nonbonding orbital (**2**). The calculated band structure of YNi_2B_2C in Figure 4 shows this result—the Y x^2–y^2 band has a minimum near –10.0 eV at Γ and rises rapidly as *k* moves away from Γ. Furthermore, for the $z^* = 0$ plane of the FBZ, this orbital is symmetric with respect to reflection in the *xy* plane of real space (**3**), while the other bands in this region of the DOS are antisymmetric. Therefore, the bottom of the Y x^2–y^2 band can "slide" upward in energy as *a* increases from right to left along the lanthanide series as the through-space Ln–Ln overlap drops.

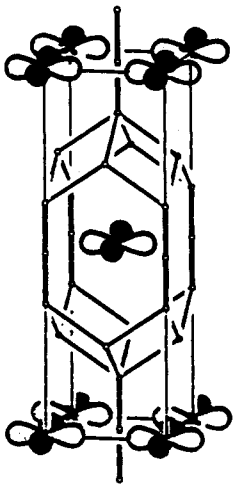

3

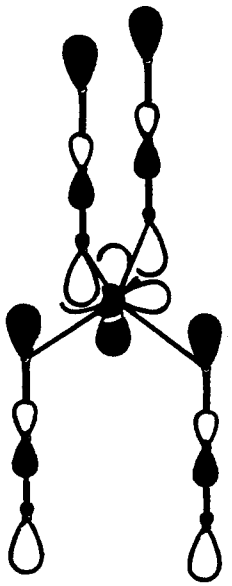

4

The band structure in Figure 4 also reveals not only narrow dispersion for the bands near the Fermi level but also that E_F lies quite close to the degenerate pair of B–C–B π nonbonding orbitals (Γ point; ca. –9.6 eV). The fourth band near E_F (Γ point; ca. –9.1 eV) contains carbon character by mixing the $2\sigma_u$ B–C–B fragment orbital with Ni 3d and 4p contributions (see **4**). The conflicting overlaps (antibonding: 3d-$2\sigma_u$; bonding: 4p-$2\sigma_u$) result in a nearly dispersionless band for much of the FBZ and a position in the total DOS close to the Fermi level. Thus, we arrive at a four-band model near the Fermi level with the following

(11) (a) Mehrotra, P. K.; Hoffmann, R. *Inorg. Chem.* **1978**, *17*, 2187. (b) Dedieu, A.; Hoffmann, R. *J. Am. Chem. Soc.* **1978**, *100*, 2074. (c) Jiang, Y.; Alvarez, S.; Hoffmann, R. *Inorg. Chem.* **1985**, *24*, 749. (d) Cui, C. X.; Kertesz, M. *Inorg. Chem.* **1990**, *29*, 2568.

(12) Miller, G. J., unpublished research. See, also: Burdett, J. K.; Canadell, E.; Miller, G. J. *J. Am. Chem. Soc.* **1986**, *108*, 6561.

(13) Cotton, F. A.; Wilkinson, G. *Advanced Inorganic Chemistry*, 4th ed.; Wiley-Interscience: New York, 1980.

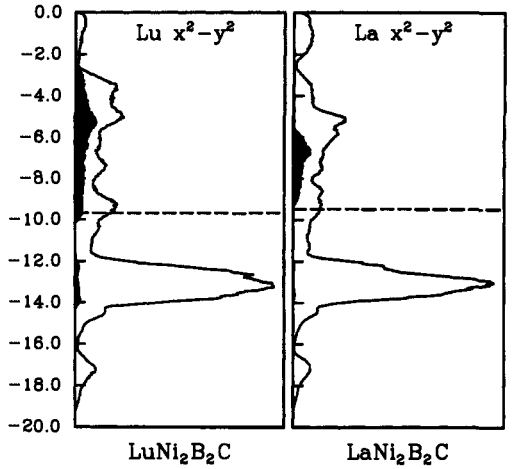

Figure 5. Total energy DOS and projection of the Ln x^2–y^2 band in $LuNi_2B_2C$ (left) and $LaNi_2B_2C$ (right). Fermi levels (–9.77 eV for Lu, –9.44 eV for La) are indicated by the dashed lines.

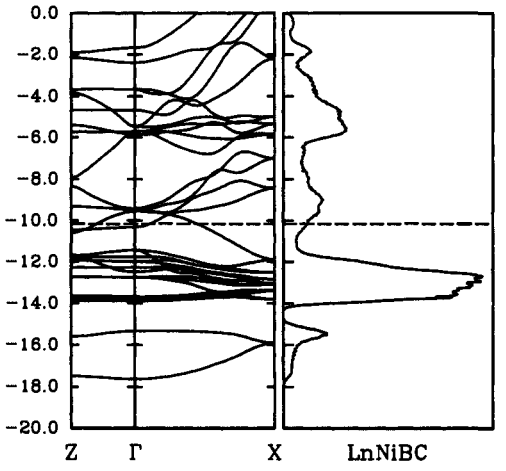

Figure 6. Total energy DOS and the energy band structure of YNiBC along two different directions of the FBZ for a simple tetragonal lattice.[14] The Fermi level (–10.18 eV) is noted by the dashed line. Γ (0,0,0), X (1/2,0,0), Z (0,0,1/2).

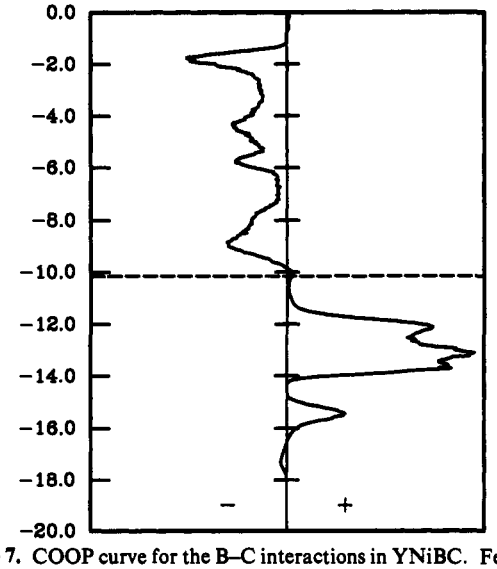

Figure 7. COOP curve for the B–C interactions in YNiBC. Fermi level is indicated by a dashed line: (+) represents bonding interactions and (–) indicates antibonding interactions. Integrated COOP value at E_F is 0.95.

features: (1) low dispersion throughout reciprocal space that leads to a local maximum in the DOS; (2) E_F lying very close to a degenerate band that is B–C nonbonding; and (3) the "σ_u" band[15] just above the Fermi level can couple to the degenerate "π_g" band[15] at E_F by a second-order Jahn–Teller mechanism[16] via a $\pi_g \otimes \sigma_u = \pi_u$ vibrational mode, i.e., a bending of the B–C–B fragment (see **5**). The dispersion characteristics along the ΓM direction, i.e., c^*, indicate that this Jahn–Teller active phonon need not be restricted to regions in reciprocal space just around $k = 0$. In particular, the Jahn–Teller mechanism appears to be especially effective because of the small energy difference between the σ_u band and the π_g band as well as the strong coupling matrix element when this bending mode is employed. Thus, the Fermi level for $LnNi_2B_2C$ falls in a region of the DOS that contains weak orbital interactions among the various components of the structure and can, therefore, be greatly affected by electron–phonon coupling. This class of superconductor shows aspects within its electronic structure of corresponding to BCS-type materials with large values of both $N(E_F)$ and V.

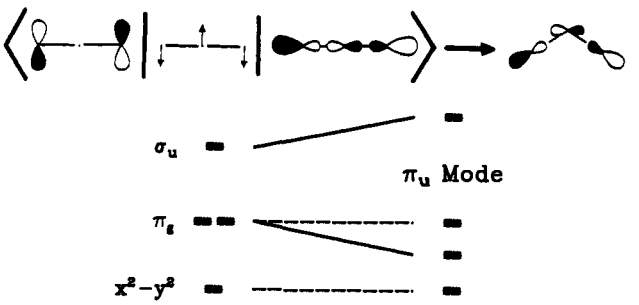

5

In addition, although our semiempirical one-electron treatment cannot treat the superconducting state appropriately,[17] we contend that the position of the lanthanide x^2–y^2 band is also a critical contributor to the observation of superconductivity. Figure 5 compares the total DOS and the x^2–y^2 projection for $LuNi_2B_2C$ and $LaNi_2B_2C$. As a increases and the 5d orbital energy of the lanthanide element rises,[18] the bottom of the x^2–y^2 band also rises and the overall bandwidth decreases. For Lu, the bottom of this band lies slightly below the calculated Fermi level, while for La, this band is above E_F. As the x^2–y^2 band becomes depleted of electrons, the B–C–B bands in this region are increasingly occupied, and according to the B–C and Ni–B overlap populations (see Figures 2 and 3), we expect the c axis length to decrease, in agreement with experiment. As we previously remarked, although the trend in c as Ln varies from Lu to La does not follow the lanthanide contraction, the total unit cell volume does increase linearly with increasing size of the Ln cation.

Another question surrounding these materials concerns the dimensionality of conductivity in the normal state of $LnNi_2B_2C$. The band structure in Figure 4 indicates three-dimensional character. Calculations using a structural model which treats the lanthanide cation as a classical ion donating three electrons while contributing no orbital components to the electronic structure of the $[Ni_2B_2C]$ substructure confirm the three-dimensional nature of the conductivity and emphasize that it is an inherent property of the $[Ni_2B_2C]$ arrangement.

Comparison with LnNiBC

The analogous phases LnNiBC (see **6**) are the next step in the series $(LnC)_n(Ni_2B_2)$[8] and *seem* to have greater anisotropy than

(14) Lax, M. J. *Symmetry Principles in Solid State and Molecular Physics*; Wiley: New York, 1974.

(15) The group of the wavevector Γ is $4/mmm$ (D_{4h}). The appropriate labels for the irreducible representations spanned by the bands in question are (i) σ_u: a_{2u}; (ii) π_g: e_g; and (iii) π_u: e_u. Labels used in the text refer to orbitals from the B–C–B fragment.

(16) Burdett, J. K. *Molecular Shapes*; John Wiley: New York, 1980.

(17) Inkson, J. C. *Many-Body Theory of Solids*; Plenum Press: New York, 1984.

(18) Structure–property correlations in cuprate superconductors are discussed by Whangbo, M.-H.; Torardi, C. C. *Acc. Chem. Res.* **1991**, *24*, 127.

Table 1. Summary of Computational Results for YNi_2B_2C and YNiBC

	YNi_2B_2C	YNiBC
E_F (eV)	-9.68	-10.17
q(Lu)	1.89	2.00
q(Ni)	10.41	10.23
q(B)	2.66	2.48
q(C)	4.98	5.29
p(B–C)	0.99	0.95
p(Ni–B)	0.17	0.16
p(Ni–Ni)	0.05	0.04
p(Y–C)	0.12	0.21 $\perp c$
		0.41 $\parallel c$

Table 2. Atomic Parameters Used in the Extended Hückel Calculations[a]

atom	orbital	H_{ii} (eV)	ζ_1	C_1	ζ_2	C_2
B	2s	-15.20	1.30			
	2p	-8.50	1.30			
C	2s	-21.40	1.63			
	2p	-11.40	1.63			
Ni	4s	-8.86	1.93			
	4p	-4.90	1.93			
	3d	-12.99	5.75	0.5817	2.20	0.5800
Y	5s	-8.13	1.74			
	5p	-5.13	1.70			
	4d	-8.32	1.56	0.8316	3.55	0.3041
La	6s	-7.67	2.14			
	6p	-5.01	2.08			
	5d	-8.21	3.78	0.7765	1.38	0.4586
Lu	6s	-8.22	1.67			
	6p	-5.22	1.67			
	5d	-8.43	2.81	0.7044	1.21	0.4880

[a] Double-ζ functions are used for the transition metals.

$LnNi_2B_2C$, because the coupling between Ni_2B_2 layers occurs through Ln–C bonds rather than B–C–B fragments. The calculated total DOS in Figure 6 shows that LnNiBC should show metallic behavior, and the band structure near E_F has significant dispersion. The Ln–C axial interactions are sufficiently strong to preclude any anisotropic conductivity, but the B–C COOP curves (see Figure 7) suggest the ionic formulation $Ln^{3+}Ni^0(BC)^{3-}$ with $(BC)^{3-}$ isoelectronic to CO, since B–C bonding is optimized at 20 electrons per formula unit. The nearly dispersionless band just below E_F along the line ΓZ (parallel to c^*) has mostly Ln x^2-y^2 character. However, the B–C interaction changes rapidly from bonding to antibonding. Therefore, since these quaternary materials do not show superconductivity, both the B–C–B nonbonding orbitals and the x^2-y^2 Ln-centered band contribute to the superconductivity in the $LnNi_2B_2C$ phases.

Table 1 summarizes the results of calculations on both $LuNi_2B_2C$ and LuNiBC. The greatest differences occur in the Y–C substructure. Both the Mulliken populations as well as Y–C overlap populations are significantly different. Moreover,

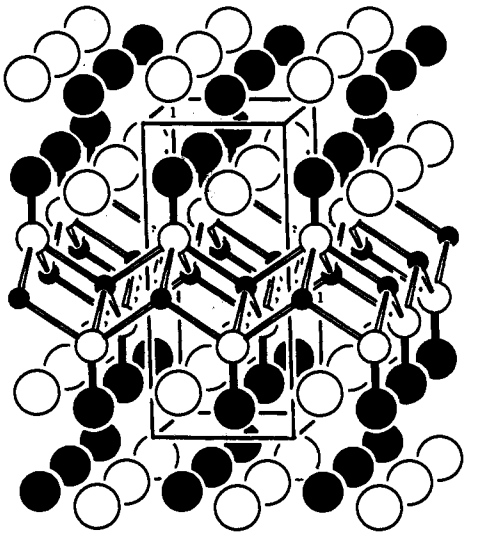

6

there is little change in the bonding within the (Ni_2B_2) layers from one structure to the other.

Summary

Band structure calculations on the series of new compounds $(LnC)_n(Ni_2B_2)$ (n = 1, 2) account well for observed trends in their structural parameters and properties. In particular, superconductivity in some of the n = 1 phases is critically dependent upon the effects of size and the nature of the local electronic structure of the B–C–B fragments. The large value of $N(E_F)$ and strong electron–phonon coupling that can arise via a second-order Jahn–Teller mechanism can both contribute to the observed T_cs. In addition, occupation of the Ln x^2-y^2 orbital, whose bandwidth is greatly affected by the a parameter, also plays a role and must be included in theories that address many-electron effects.

Appendix

All electronic structure calculations were of the extended Hückel tight-binding type.[2] The observed lattice parameters of $LuNi_2B_2C$, YNi_2B_2C, $LaNi_2B_2C$, and LuNiBC and atomic positions were set by the data reported for $LuNi_2B_2C$.[8] Atomic orbital parameters for all atoms, listed in Table 2, and charge iteration parameters for Y and Ni were taken from standard sources.[19] DOS and COOP curves were evaluated using special k-points sets,[20] and tight-binding overlaps were included within three neighboring unit cells along every translation vector.

(19) (a) Clementi, E.; Roetti, C. *At. Data Nucl. Data Tables* **1974**, *14*, 177. (b) Baranovskii, V. I.; Nikolskii, A. B. *Teor. Eksp. Khim.* **1967**, *3*, 527.
(20) Chadi, D. J.; Cohen, M. L. *Phys. Rev. B* **1973**, *8*, 5747.